Article

Flood Monitoring Using Sentinel-1 SAR for Agricultural Disaster Assessment in Poyang Lake Region

Hengkai Li [1], Zikun Xu [1], Yanbing Zhou [2,*], Xiaoxing He [1] and Minghua He [1]

1   Jiangxi Province Education Department, School of Civil and Surveying & Mapping Engineering, Jiangxi University of Science and Technology, Ganzhou 341000, China; giskai@jxust.edu.cn (H.L.); 6120210132@mail.jxust.edu.cn (Z.X.); xxh@jxust.edu.cn (X.H.); 6720200506@mail.jxust.edu.cn (M.H.)
2   Information Technology Research Center, Beijing Academy of Agriculture and Forestry Sciences, Beijing 100097, China
*   Correspondence: zhouyb@nercita.org.cn

Abstract: An extensive number of farmlands in the Poyang Lake region of China have been submerged due to the impact of flood disasters, resulting in significant agricultural economic losses. Therefore, it is of great importance to conduct the long-term temporal monitoring of flood-induced water body changes using remote sensing technology. However, the scarcity of optical images and the complex, fragmented terrain are pressing issues in the current water body extraction efforts in southern hilly regions, particularly due to difficulties in distinguishing shadows from numerous mountain and water bodies. For this purpose, this study employs Sentinel-1 synthetic aperture radar (SAR) data, complemented by water indices and terrain features, to conduct research in the Poyang Lake area. The results indicate that the proposed multi-source data water extraction method based on microwave remote sensing data can quickly and accurately extract a large range of water bodies and realize long-time monitoring, thus proving a new technical means for the accurate extraction of floodwater bodies in the Poyang Lake region. Moreover, the comparison of several methods reveals that CAU-Net, which utilizes multi-band imagery as the input and incorporates a channel attention mechanism, demonstrated the best extraction performance, achieving an impressive overall accuracy of 98.71%. This represents a 0.12% improvement compared to the original U-Net model. Moreover, compared to the thresholding, decision tree, and random forest methods, CAU-Net exhibited a significant enhancement in extracting flood-induced water bodies, making it more suitable for floodwater extraction in the hilly Poyang Lake region. During this flood monitoring period, the water extent in the Poyang Lake area rapidly expanded and subsequently declined gradually. The peak water area reached 4080 km^2 at the height of the disaster. The severely affected areas were primarily concentrated in Yongxiu County, Poyang County, Xinjian District, and Yugan County.

Keywords: Sentinel-1; water extraction; flood disaster; decision tree; random forest; improved U-Net

1. Introduction

Flood disasters are one of the major catastrophes in China, causing significant losses to the national agricultural economy each year, primarily by reducing the yields of food crops. Numerous crops thrive in water-rich environments and are commonly cultivated near rivers and lakes, and as a consequence, the widespread inundation of farmlands is a direct impact of floods on agricultural production. The flood season in southern China typically coincides with critical stages in the rice cultivation process, such as the heading and harvesting of early-season rice, the field management of mid-season rice, and the transplanting of late-season rice seedlings. This situation exerts adverse effects on rice production and can even lead to complete crop failure. According to the "2020 Annual Report on National Natural Disasters" issued by the Chinese Ministry of Emergency Management, the floods occurring in China during 2020 destroyed close to 3869 hectares

of crops in July alone, causing direct economic losses of CNY 1097.4 billion [1]. Among them, the catastrophic floods caused by heavy rainfall in the Yangtze and Huai River basins were one of the top 10 major disasters in China in 2020 [2]. The accurate acquisition of temporal and spatial distribution information of floodwater can aid in dynamically monitoring floods, provide technical support for flood monitoring in the southern hilly areas of China, and act as a reference for the adjustment and optimization of agricultural production structures and food security in the future.

Satellite remote sensing technology is gradually replacing manual monitoring methods due to characteristics including coverage of large measurement areas, non-intrusive measurements, and low cost. In particular, optical remote sensing is widely used due to its rich data sources that can be applied to calculate numerous spectral indices for water bodies, including the normalized difference water index (NDWI) [3], super green water index [4], vegetation red-edge water index [5], etc. However, the cloudy and rainy conditions that frequently occur during the flood season in southern China adversely affect the performance of optical remote sensing sensors, making it difficult to obtain stable and usable optical images for flood monitoring [6]. As a result, the disaster assessment is often limited to comparing pre-disaster and post-disaster images, which may not effectively capture the entire process of prolonged and continuous floods in southern China.

The development of microwave remote sensing, particularly the release of free Sentinel-1 SAR data, has provided new data sources for flood monitoring. For example, Zeng et al. [7], Chen and Jiang [8], and Jia et al. [9] utilized microwave data to extract water body information using methods such as simple thresholding, change detection combined with thresholding, and the Sentinel-1 dual-polarized water index (SDWI). Additional research, both domestic and international, has proposed related methods including Otsu optimal threshold segmentation [10] and object-based approaches [11]. However, these methods primarily focus on enhancing water body characteristics while neglecting the influence of mountain shadows formed by the side-looking imaging of Sentinel-1 satellites. Mountain shadows and water bodies have similar backscattering coefficients, resulting in a similar dark tone in Sentinel-1 SAR images, making it challenging to distinguish between the two during the extraction of water bodies. In regions with frequent floods, such as the southern hilly areas of China, the terrain is undulating, and mountain shadows are prevalent. Thus, there is an urgent need to address the rapid and accurate extraction of flood-affected areas by accounting for the characteristic topography and water body attributes of these southern hilly regions.

In an attempt to acutely distinguish between shadows and water bodies in mountainous areas, Yang et al. [12] simulated radar images using terrain data and removed the shadows that were falsely identified as floodwater bodies, achieving the semi-automatic and accurate extraction of large-scale floodwater bodies. Therefore, this study focuses on removing mountain shadows based on terrain features. More specifically, decision tree nodes are introduced to rapidly assess the impact of terrain features on mountain shadows. Decision trees offer several advantages in binary classification, including fast calculation, simple principles, and accurate results, and thus they are widely used in water body extraction applications [13,14]. In recent years, with the continuous development of artificial intelligence algorithms, machine learning methods such as maximum likelihood, random forest, and support vector machines have been extensively applied in remote sensing research. Among them, the random forest method demonstrates high classification accuracy, a fast prediction speed, and the ability to handle multi-dimensional data [15–17]. Li et al. employed the random forest method based on multi-source data for land-use classification in the southern hilly mountains, effectively addressing the low classification accuracy caused by mountain shadows. Deep learning can fully explore the feature information in remote sensing images and has gradually become more popular in water body extraction applications [18–20]. Among the deep learning models, U-Net has proven to exhibit a high extraction accuracy and minimal spatial resolution losses [21,22], making it suitable for precise water body extraction. However, current research on deep learning-based water

body extraction methods primarily focuses on optical remote sensing, while relatively few studies have been conducted on microwave remote sensing [23].

This study employs the decision tree, random forest, and improved U-Net algorithms for water body extraction using the flood disaster in the Poyang Lake area as a case study and Sentinel-1 SAR images from 30 September 2019 as the data source. A comparison of the shadow removal effect and accuracy of the water body extraction results for each method is performed to select the most suitable approach for floodwater extraction in the Poyang Lake region. The selected method is then used to analyze the spatiotemporal distribution of floodwater bodies in the Poyang Lake area from June to August 2020. This work provides valuable insights for the planning of agricultural infrastructure.

2. Study Area and Data Sources

2.1. Overview of the Study Area

Located in the northern part of Jiangxi Province, China, Poyang Lake (between 28°22′–29°45′N and 115°47′–116°45′E) is the largest freshwater lake in the country. Within Jiangxi, the total area of the county-level regions through which Poyang Lake flows is approximately 22,300 km^2, including 11 counties and cities such as Lianxi District, Hukou County, Lushan City, Poyang County, and Nanchang County (Figure 1). The surrounding area of Poyang Lake is characterized by complex land cover and significant topographical variations. The dominant landform type is hilly terrain, accounting for about 78% of the total area, followed by plains and hillocks (approximately 12.1% of the total), and water bodies (covering about 9.9%). Poyang Lake is located in a low-lying area and is influenced by the East Asian monsoon, with concentrated rainfall during the summer season. As a result, from July to September, the lake's water area rapidly expands during the flood season, and the limited drainage capacity, combined with its unique relationship with the Yangtze River, often leads to frequent flood disasters. Since 1949, there have been over 20 recorded major flood events in the area [24].
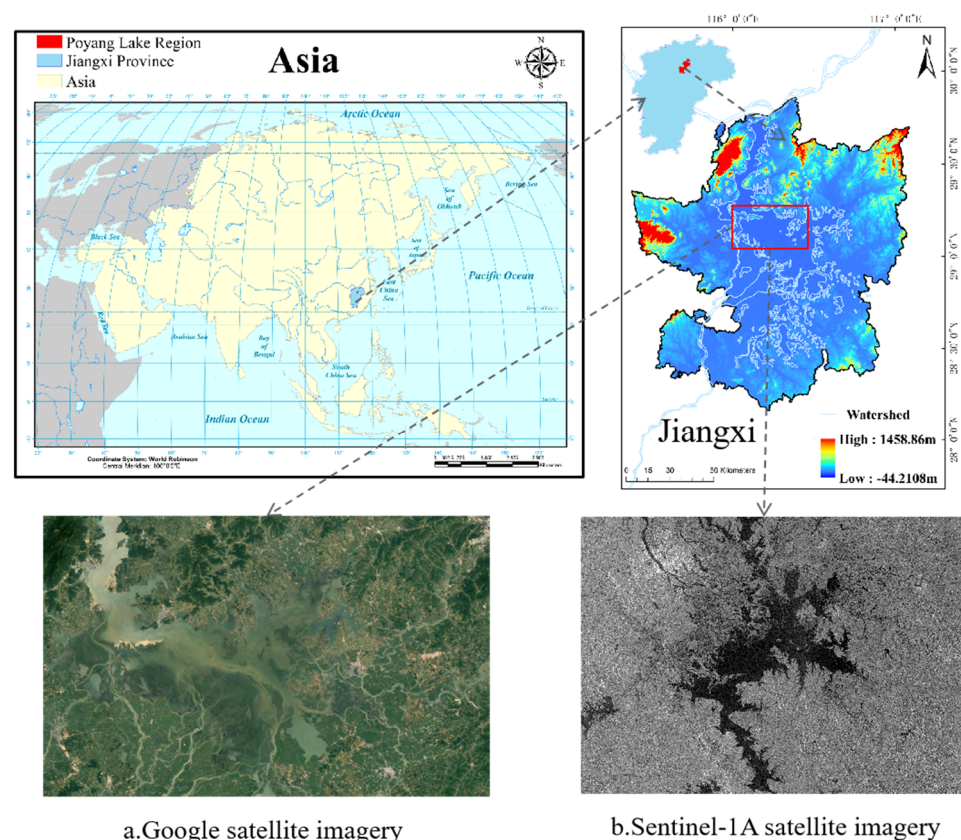

Figure 1. The location of Poyang Lake.

2.2. Data Source

Sentinel-1 SAR satellite imagery was downloaded from the European Space Agency's official website (http://scihub.copernicus.eu (accessed on 27 July 2023)), and corresponding precise orbit data were obtained from the website (https://s1qc.asf.alaska.edu/ (accessed on 27 July 2023)). Moreover, 30 m resolution SRTM-1 Digital Elevation Model (DEM) data were downloaded from the Geospatial Data Cloud Platform (http://www.gscloud.cn (accessed on 27 July 2023)). Supplementary data included vector maps of the administrative divisions of the counties in the study area, water level data, and Google Earth imagery.

Sentinel-1 SAR satellite imagery has a resolution of 10 m and comes in four imaging modes, with a maximum swath width of 400 km. These images are favored by many researchers due to their free availability and high resolution, and they have been widely applied in various fields. The VV (vertical-vertical) and VH (vertical-horizontal) polarized bands of Sentinel-1 imagery are typically used for water body extraction. Hence, we employed the Ground Range Detected Product (GRD) data from the Interferometric Wide Swath (IW) mode. Google Earth imagery was available only for 4 October 2019 in the study area, and thus a Sentinel-1B SAR image from 30 September 2019 was selected to construct the water body extraction method. Another Sentinel-1B SAR image from the flood period in 2020 was selected for flood disaster analysis in the study area. Detailed image information is presented in Table 1. The DEM dataset was used to remove misidentifications caused by mountain shadows, while the Google Earth high-resolution imagery and water level data were employed for the sample selection and flood disaster analysis, respectively.

Table 1. Sentinel-1 SAR image data information.

Data	Platform	Type	Polarization Mode
30 September 2019	Sentinel-1 B	GRD	VV, VH
20 June 2020	Sentinel-1 B	GRD	VV, VH
2 July 2020	Sentinel-1 B	GRD	VV, VH
14 July 2020	Sentinel-1 B	GRD	VV, VH
26 July 2020	Sentinel-1 B	GRD	VV, VH
7 August 2020	Sentinel-1 B	GRD	VV, VH
19 August 2020	Sentinel-1 B	GRD	VV, VH

2.3. Data Preprocessing

The data preprocessing steps included track correction, radiometric calibration, filtering, terrain correction, decibelization, mosaic creation, and clipping. Radiation calibration converts the intensity value of the image into the backscattering coefficient using the following conversion relationship:

$$\sigma^0 = \frac{A^2}{K}\theta \tag{1}$$

where σ^0 is the backscattering coefficient; A is the DN value of the original image; K is the absolute scaling factor; and θ is the angle of incidence.

The filtering process utilizes the Refined Lee filter, which effectively eliminates speckle noise while preserving the edge information of features [25]. The terrain correction combines SRTM-1 DEM data obtained through bilinear interpolation and corrects the geometric distortion caused by terrain using the distance Doppler algorithm. The conversion to decibels involves transforming the backscatter coefficients of the image into logarithmic form, which is more conducive to reflecting the differences in radar intensity.

3. Methods

3.1. Image Feature Extraction

(1) Radar image feature

The VV and VH backscatter coefficients are the main data features extracted from the Sentinel-1 SAR image data for water body extraction in this study. They provide different

scattering characteristics between various objects, enabling the enhancement of floodwater identification by distinguishing the different scattering properties of water and non-water bodies in radar signals. The two backscatter coefficients are determined as follows:

$$\sigma_{VV}(\text{db}) = 10 * \log_{10}(\sigma_{VV}) \tag{2}$$

$$\sigma_{VH}(\text{db}) = 10 * \log_{10}(\sigma_{VH}) \tag{3}$$

where $\sigma_{VV}(\text{db})$ and $\sigma_{VH}(\text{db})$ are the backscatter coefficients, and σ_{VV} and σ_{VH} are the pixel values of the two polarized images.

(2)   Sentinel-1 dual-polarized water index

Among the main water body extraction methods used for Sentinel-1 SAR images, threshold segmentation is simple, fast, and can rapidly provide valuable information for flood disaster assessments. However, the "double peaks" feature of a single band is not distinct, making it challenging to obtain accurate thresholds and consequently resulting in suboptimal water body extraction results. The SDWI, proposed by Jia et al. (2019), is inspired from the normalized difference vegetation index (NDVI) and NDWI, and is calculated as follows:

$$K_{\text{SDWI}} = \ln(10 \times VV \times VH) \tag{4}$$

where K_{SDWI} is the SDWI, and VV and VH represent the VV and VH backscatter coefficients, respectively.

The SDWI multiplies the data from two polarized bands of the Sentinel-1 SAR satellite, enhancing the characteristics of water bodies while attenuating the features of soil and vegetation, thereby obtaining distinct "double peaks" that are effective for water body extraction. Figure 2 presents the pixel histogram of the preprocessed SAR image after SDWI calculation, revealing clear peaks and valleys. The lowest value of the valley, −7.4605, represents the threshold for the SDWI threshold segmentation method. In this study, the decision tree method uses this threshold as the root node, enabling the preliminary coarse extraction of water bodies in the study area.
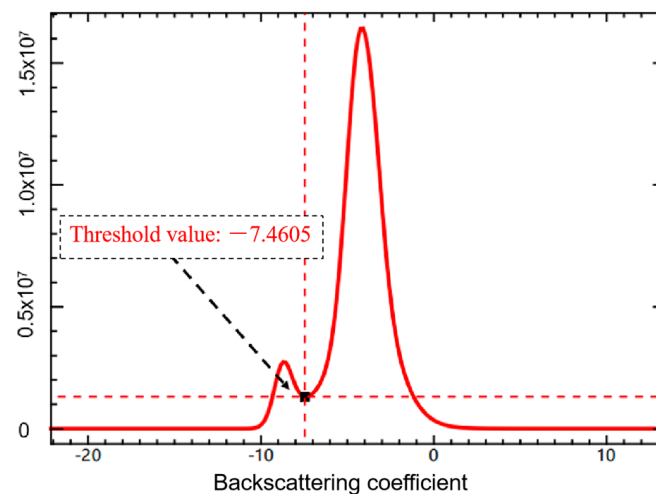

Figure 2. Pixel histogram of SDWI images in the study area.

(3)   Topographic feature

The SDWI values for water bodies and mountain shadows are similar in the water body class, making it difficult to distinguish between them using just this index. To remove the mixed mountain shadows from the extracted water bodies, we incorporate terrain features such as elevation and slope into the decision tree and random forest decision tree nodes to suppress the false positives. By combining high-resolution Google Earth

imagery from 4 October 2019, the coarse-extracted water bodies are visually examined, identifying the main areas of misclassification between water bodies and shadows. The elevation and slope information for these regions are then obtained to establish approximate threshold ranges to differentiate water bodies from shadows. Precise threshold values that effectively remove shadows are calculated using iterative analysis, with 300 m determined for elevation and 18 for slope. The elevation and slope information are derived from the SRTM-1 DEM data through terrain analysis processing.

3.2. Water Extraction Method

(1) Decision Tree

The decision tree (DT) model recursively partitions a set of training data into subsets with the same classification features by testing a single feature at the root node or multiple features at the leaf nodes [26]. This model is effective in solving binary classification problems. It quickly and intuitively captures the impact of each feature on the classification categories. Therefore, in this study, the DT method was initially applied to water body extraction to assess the influence of terrain features on mountain shadows. The proposed method considers the actual conditions of the study area, combining features such as the SDWI, elevation, and slope for water body extraction in the Poyang Lake area.

(2) Random Forest

The random forest (RF) algorithm is a classifier based on the Bagging ensemble learning theory [27]. This algorithm builds a series of decision trees by constructing different sample training sets and subsequently integrates all classification voting results obtained by majority voting decisions after K rounds of training. Finally, according to the principle of minority obedience to the majority, the category with the most votes is designated as the final output. The final classification decision is described as follows:

$$H(x) = arc\max_{Y} \sum_{i=1}^{K} I(h_i(x) = Y) \tag{5}$$

where $H(x)$ is the final classification result of random forest result; $h_i(x)$ denotes the classified results for a single decision tree; Y is the output variable; and $I()$ is the characteristic function.

This approach is independent of prior knowledge from interpreters and can thus handle high-dimensional and complex datasets, with extensive applications in land use classification and landslide hazard assessments, amongst other fields [28,29]. In this study, based on Sentinel-1 SAR imagery and DEM data, we selected three types of indicators for water body extraction in the random forest model, namely, radar feature variables, water index variables, and terrain feature variables.

(3) Improved U-Net

The U-Net network model, named after its U-shaped structure, is an improved end-to-end architecture based on the Fully Convolutional Network (FCN) framework [30]. This model can effectively fuse high-level semantic information and shallow features, leveraging context information and detail features to obtain more accurate feature maps [31]. However, the original U-Net model only uses three-channel imagery as the input and does not fully consider the terrain and landform characteristics within the study area. To address this limitation, we enhanced the model by modifying the image input to six channels, enabling the model to simultaneously extract radar features, water indices, and terrain characteristics. Moreover, to explore deep semantic information in the six-channel imagery, we replaced the original feature extraction network of the model with the deeper VGG16 convolutional neural network. We also incorporated a channel attention mechanism during the downsampling process of the convolutional network (Figure 3) to update the model's attention weights for different channels and further improve the segmentation performance. Finally, to better distinguish water body boundaries, we modified the model's loss function

by introducing the Dice coefficient in addition to the Cross-Entropy Loss, creating the Dice Loss to assist the classifier and achieve better segmentation results. Based on these improvements, we obtained the enhanced U-Net, denoted as the Channel Attention U-Net (CAU-Net) semantic segmentation model for water body extraction in the Poyang Lake area. Figure 4 presents the structure of the optimized model.
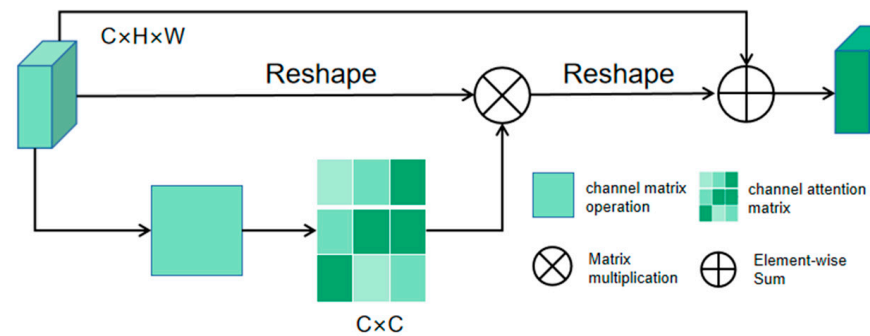

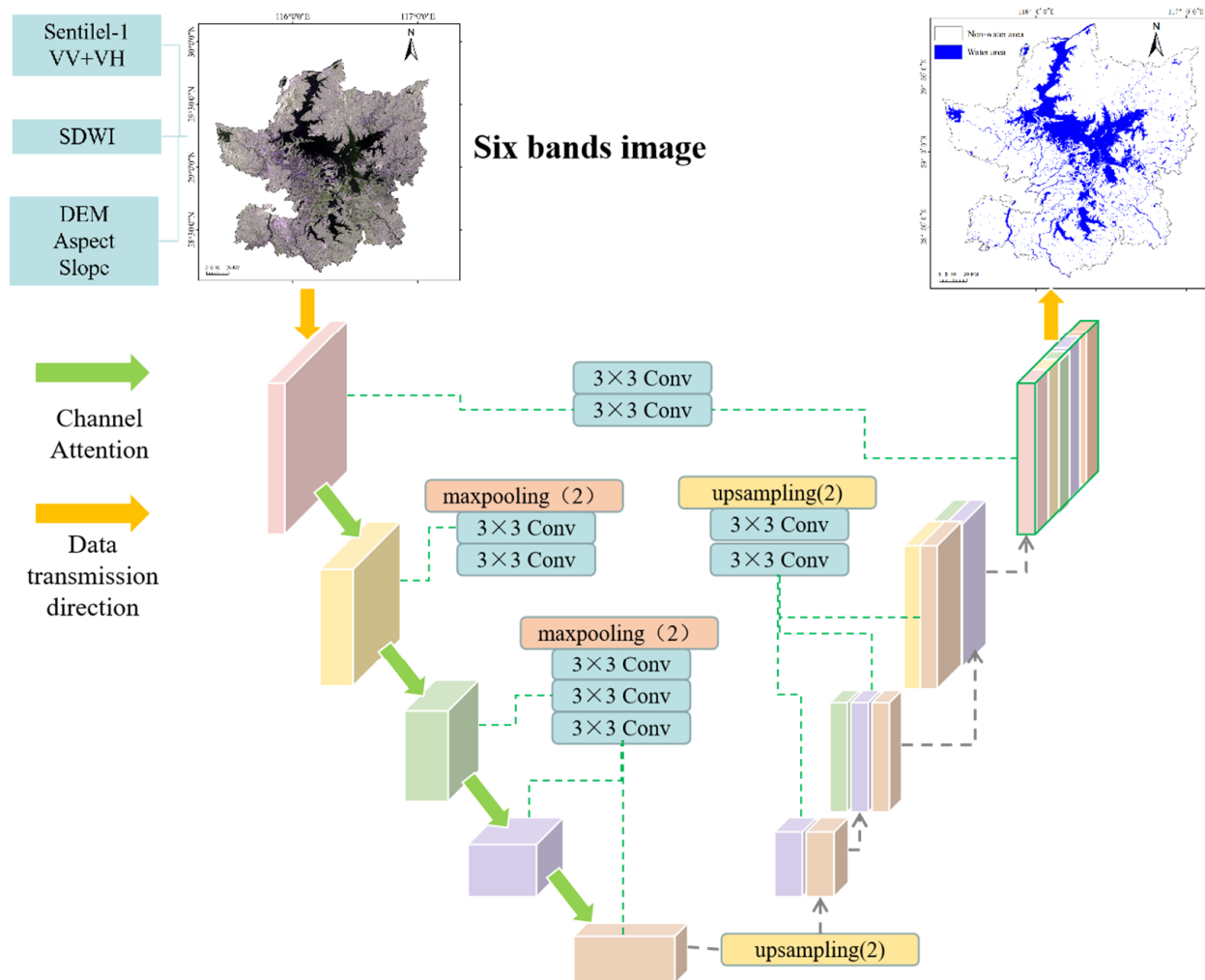
Figure 3. Channel attention mechanism.

Figure 4. Model structure.

The CAU-Net model is implemented in the TensorFlow deep learning framework. To enhance the model training stability, improve generalization ability, and accelerate training speed, this study utilized the cosine annealing learning rate decay mechanism to adjust the

learning rate during the model training process. The initial learning rate was set to 10-4, and it continuously decayed according to formula 6 during the training process, enabling the model to descend stably in the correct gradient direction. The model hyperparameters were adjusted using the Adaptive Moment Estimation (Adam) optimizer, aiming to improve the model's convergence.

$$\eta_t = \eta_{\min} + \frac{1}{2}(\eta_{\max} - \eta_{\min})(1 + \cos(\frac{T_{cur}}{T_{\max}}\pi)) \tag{6}$$

where $\eta_{\max}$ is the maximum learning rate; $\eta_{\min}$ is the minimum learning rate; T_{cur} is the current round; and $T_{\max}$ is half a cycle.

In order to increase the accuracy of the model water boundary segmentation, the Loss function used in the training process was constructed as Dice_Loss by introducing the Dice coefficient based on Cross Entropy Loss. Dice_Loss is expressed as follows:

$$Dice\_Loss = 1 - \frac{2\sum_{i=1}^{n} y_i a_i}{\sum_{i=1}^{n} y_i + \sum_{i=1}^{n} a_i} \tag{7}$$

where n represents the total number of test data; y represents the truth value; and a represents the predicted value.

During the model training process, the goodness-of-fit function of the model stabilized and converged when the number of iterations was close to 20. The training model obtained in the previous step was used for the extraction of water bodies in the Sentinel-1B SAR image of the study area.

3.3. Sample Selection

The number, distribution, and representativeness of training samples can significantly impact the accuracy of the water body extraction [32]. In this study, water bodies were treated as a binary classification problem, dividing the study area into two classes: water and non-water. Water bodies exhibit color differences in shallow and deep water areas, and thus a suitable number of samples were selected for each category while ensuring a diverse representation of non-water land cover types. For the decision tree and random forest methods, training samples were generated through visual interpretation and random sampling from Google Earth high-resolution imagery, resulting in a total of 1440 sample points that were split into training and validation sets at a ratio of 7:3.

For the CAU-Net method, a dataset must be constructed to train the model, considering the differences between water bodies and mountain shadows. The dataset was synthesized from six-band images including VV and VH radar features, SDWI data, elevation, slope, and aspect as the bands. The study area was covered by a large Sentinel-1 SAR image. In order to incorporate different water body types from various regions, six representative sub-regions were selected, including mountainous regions, flatlands (including urban areas), mountainous regions with rivers, flatlands with lakes, croplands with lakes, and flatlands with various types of water bodies (Figure 5). The images of these regions were batch-cropped to 256 × 256 pixels for model training and were manually labeled using the Labelme plugin to obtain the corresponding water body distribution labels. A total of 409 images were used to construct the water body distribution dataset, and were divided into training and validation sets at 4:1 ratio. During the training, data augmentation techniques, such as horizontal and vertical flipping, cropping, and scaling, were applied to enhance the model's generalization ability and prevent overfitting.
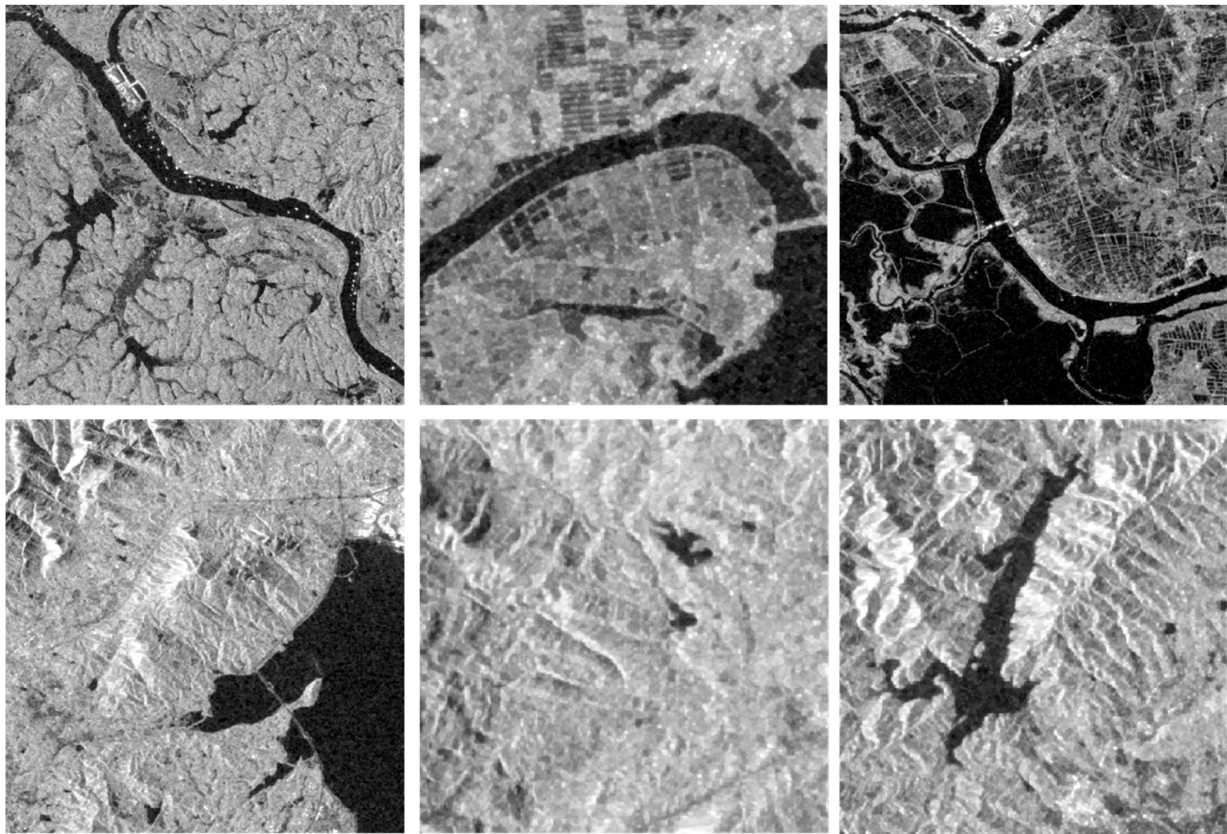
Figure 5. Typical area in the study area.

3.4. Accuracy Evaluation

In order to compare the extraction effects of different extraction methods on flood-affected water bodies, the accuracy was evaluated using two indexes, namely the overall accuracy (OA) and Kappa coefficient. Both indexes are calculated based on the confusion matrix of the extracted results as follows:

$$OA = \frac{\sum_{i=1}^{\kappa} x_{ii}}{N} \tag{8}$$

$$\text{Kappa} = \frac{N\sum_{i=1}^{k} x_{ii} - \sum_{i=1}^{k} x_{i+}x_{+i}}{N^2 - \sum_{i=1}^{k} x_{i+}x_{+i}} \tag{9}$$

where N is the total number of samples; K is the total class number; x_{ii} is the number of samples assigned to the correct category; and x_{+i} and x_{i+} are the true number of Class i samples and the predicted number of Class i samples, respectively.

4. Results

In order to compare the three water extraction methods proposed in this study, a detailed comparison was conducted by qualitatively evaluating the effectiveness of the shadow removal based on the SDWI threshold method. Furthermore, real water samples were visually interpreted from Google Earth imagery and used to construct confusion matrices with the water extraction results obtained from the four methods. This facilitated a quantitative assessment of the water extraction accuracy. Through both qualitative and quantitative analyses, the most suitable water extraction method for the Poyang Lake region was ultimately determined.

4.1. Qualitative Comparison of Water Extraction Results

Figure 6 presents the water extraction results determined by fusing the pre-processed Sentinel images with DEM data and subsequently applying the SDWI threshold approach and the three methods proposed in this study. All four methods are observed to roughly outline the water bodies in the Poyang Lake area over a large scale.
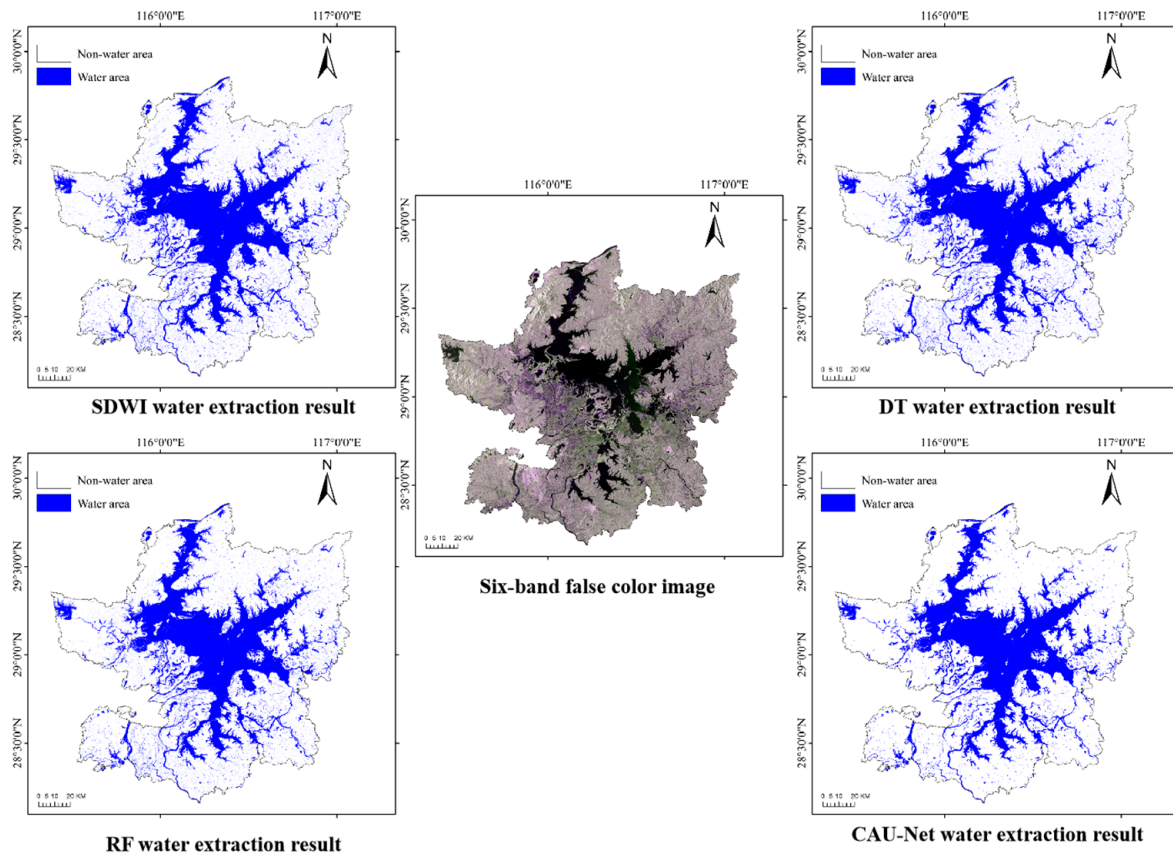

Figure 6. Results of water extraction by different methods.

In order to provide a more intuitive demonstration of the differences between the methods, we selected several typical water extraction results within the study area for a detailed comparative analysis. Figure 7 depicts the results. The water body extraction performance is observed to vary across the methods. The extraction of the SDWI method is fast and simple, yet it is influenced by various factors such as image noise and terrain, leading to suboptimal results with a significant amount of scattered misclassified water bodies. Following the incorporation of the terrain features, the decision tree and random forest methods exhibit improvements via the reduction in misclassified water bodies. However, their extraction of water body boundaries still remains relatively coarse. In comparison, the proposed CAU-Net method effectively mitigates the impact of image noise and terrain factors, greatly minimizing the misclassification of water bodies. The second row of Figure 7 reveals the presence of noise points generated due to water surface reflection. The SDWI, decision tree, and random forest methods are heavily affected by this noise, resulting in the misclassification of water bodies in the noisy regions as non-water bodies. In contrast, CAU-Net effectively suppresses the influence of this background noise. In particular, the analysis of neighboring pixels around the noise points using convolutional neural networks greatly reduces the misclassification of water bodies.
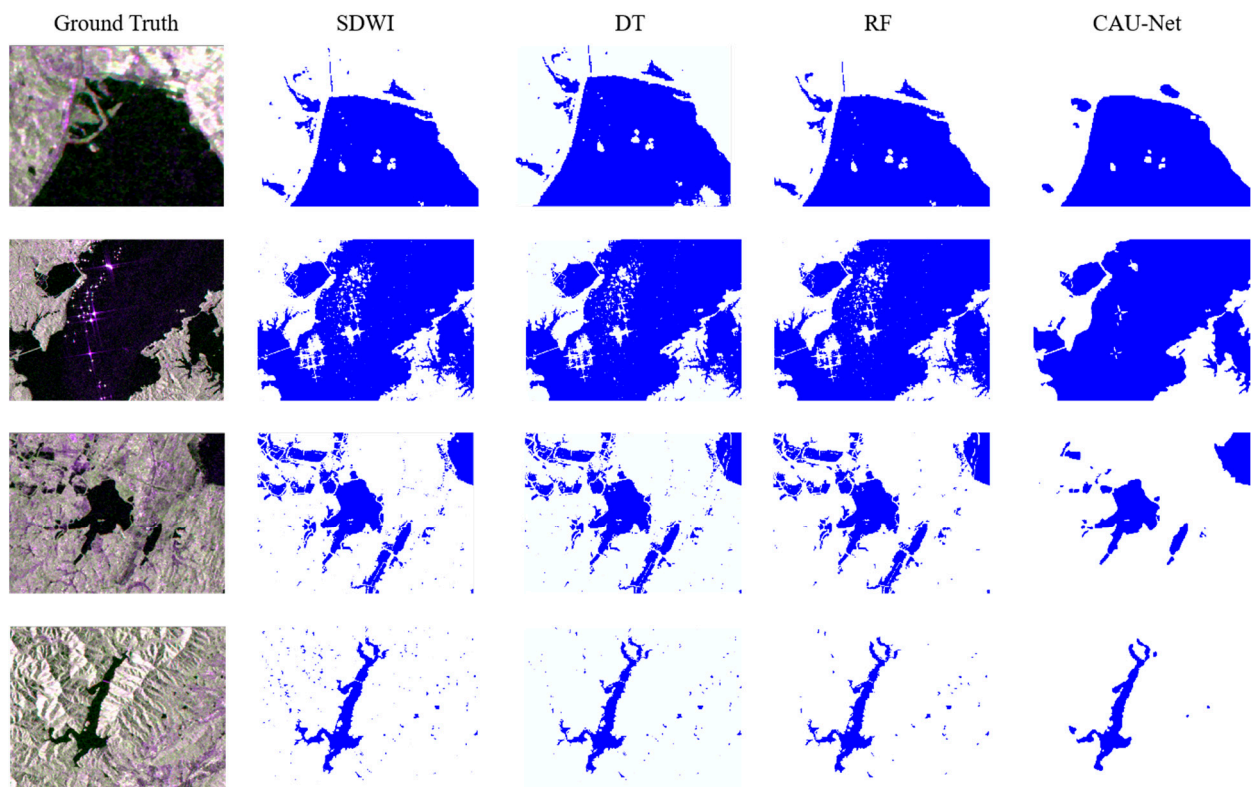
Ground Truth	SDWI	DT	RF	CAU-Net

Figure 7. Water extraction results of different methods in typical areas.

The fourth row in Figure 7 depicts a typical area of high hills within the study region, vividly illustrating the impact of each method in suppressing mountain shadows. The SDWI method, which does not account for mountain shadow effects, is observed to greatly misclassify mountain shadows as water bodies in high hill terrain. The decision tree method, which is built upon SDWI threshold segmentation and incorporates terrain features, demonstrates a fast extraction speed with a certain level of shadow suppression in hilly areas. The random forest method has a strong applicability to high-dimensional datasets and effectively eliminates misclassified mountain shadows by incorporating the water index (SDWI) and terrain features as well as the original Sentinel polarization characteristics. When incorporating terrain features as training data for multi-band remote sensing images, the CAU-Net method extensively extracts feature information from the remote sensing images. The resulting water body extraction greatly suppresses the influence of mountain shadows, yielding accurate extraction results.

4.2. Quantitative Comparison of Water Extraction Results

In order to quantitatively compare the extraction accuracy of the various extraction methods, this study conducts a comprehensive analysis using two metrics, namely, the OA and Kappa coefficient. The CAU-Net model proposed in this study demonstrates a strong performance. Compared to the traditional methods of threshold segmentation, decision tree, and random forest in machine learning, CAU-Net significantly improves the accuracy of water body extraction. More specifically, it achieves an impressive OA of 98.71% and a Kappa coefficient of 0.97, both of which outperform the comparative methods. Furthermore, using the same six-band image as input to train the data, the OA and Kappa coefficient of CAU-Net increase by 0.12% and 0.02, respectively, compared to the U-Net model without the attention mechanism. This indicates that the method proposed in this study improves on the U-Net model for water body extraction.

Following this, to investigate the impact of mountain shadows on the accuracy of water body extraction, this study selected two typical areas: (i) a hilly region around Lushan

City, which has relatively high average altitude and significant terrain undulations; and (ii) a low hilly region at the border area between Poyang and Duchang counties, with a relatively low average altitude but still exhibits some terrain undulations. A total of 188 and 197 sample points were evenly selected for validation in the two respective areas. Table 2 reports the accuracy of different water body extraction methods in these two typical areas.

Table 2. The extraction accuracy of each method in different terrain.

Landform	Evaluation Index	SDWI	DT	RF	CAU-Net
High hill	OA	89.36%	95.87%	96.19%	96.45%
	Kappa	0.87	0.89	0.89	0.91
Low hill	OA	91.48%	94.69%	95.18%	95.11%
	Kappa	0.87	0.88	0.89	0.89

Compared to the SDWI threshold method, in the high hill area, all three experimental methods showed a significant improvement in accuracy. More specifically, the OA increased by 6.51%, 6.83%, and 7.09% respectively, while the Kappa coefficient increased by 2.43%, 2.57%, and 4.57%. Improvements in accuracy were also observed in the low hill area, despite the lower level of mountain shadows. The OA increased by 3.21%, 3.70%, and 3.63% respectively, and the Kappa coefficient increased by 1.04%, 2.19%, and 1.68%. Comparing the accuracy of the experimental approaches reveals that the decision tree, random forest, and CAU-Net methods are able to suppress shadows at varying extents, effectively enhancing the accuracy of water body extraction.

4.3. Analysis of Flood Disaster in Poyang Lake

The comparison of the water body extraction results using the three methods indicates that both the SDWI method and CAU-Net can achieve the desired accuracy while ensuring timeliness. Therefore, CAU-Net is chosen as the optimal water body extraction method. Based on CAU-Net, this study utilizes the deep learning model obtained earlier to predict the water body extent during the flood period from June to August 2020 using Sentinel-1B imagery captured every 12 days. Figure 8 presents the resulting maps of the water body during the six periods.

Due to the influence of heavy rainfall over several days, the water level in the Five Rivers of Jiangxi Province rose rapidly at the end of June. From 4 to 11 July, the water level in the Poyang Lake area increased by more than 0.4 m per day for 8 consecutive days, resulting in a total of 12 numbered flood events. According to Table 3, all five key river water level stations in the Poyang Lake area exceeded the warning level during this flood disaster and reached their highest levels around 12 July. Among them, the iconic water level station, Xingzi Station, reached a record high of 22.63 m, surpassing the 1998 flood level by 13 cm and exceeding the historical extreme value.

Table 3. Flood characteristic values of water level stations of key rivers in Poyang Lake in 2020.

	Gauging Station	Highest Water Level/m	Warning Water Level/m	Occurrence Time
1	Hukou	22.49	19.50	12 July 2020
2	Xingzi	22.63	19.00	12 July 2020
3	Yongxiu	23.63	20.00	11 July 2020
4	Duchang	22.42	19.00	11 July 2020
5	Poyang	22.75	19.50	12 July 2020

The total area of the study region is 24,279 km^2. Figure 9 presents the water body areas for each period from June to August 2020. The results indicate that the water body area in the study region was only 2639 km^2 on 20 June, reaching its maximum value of 4080 km^2 on 14 July and subsequently decreasing to 3596 km^2 on 19 August. Due to the existence of flood

control embankments and low-lying areas, the change in the water body area lags behind the water level. This indicates that the maximum water body area obtained in this study is consistent with the time of the highest water level. The submerged water body area in the study area initially expanded rapidly and subsequently exhibited a slow recession during the entire flood period. At turning point 1 (2 July), the study area experienced continuous heavy rainfall, and the submerged water body area rapidly expanded, increasing by a total of 1441 km^2 during the rising period. At turning point 2, when the rainfall almost stopped and the floodwaters ceased to rise, the submerged water body slowly receded, decreasing by a total of 484 km^2 during the recession period. The rapid expansion of the floodwater in the study area placed significant pressure on the relevant departments of Jiangxi Province to respond promptly with flood control and disaster relief measures. Furthermore, the slow recession of the floodwaters posed considerable challenges for post-disaster rescue and recovery efforts.
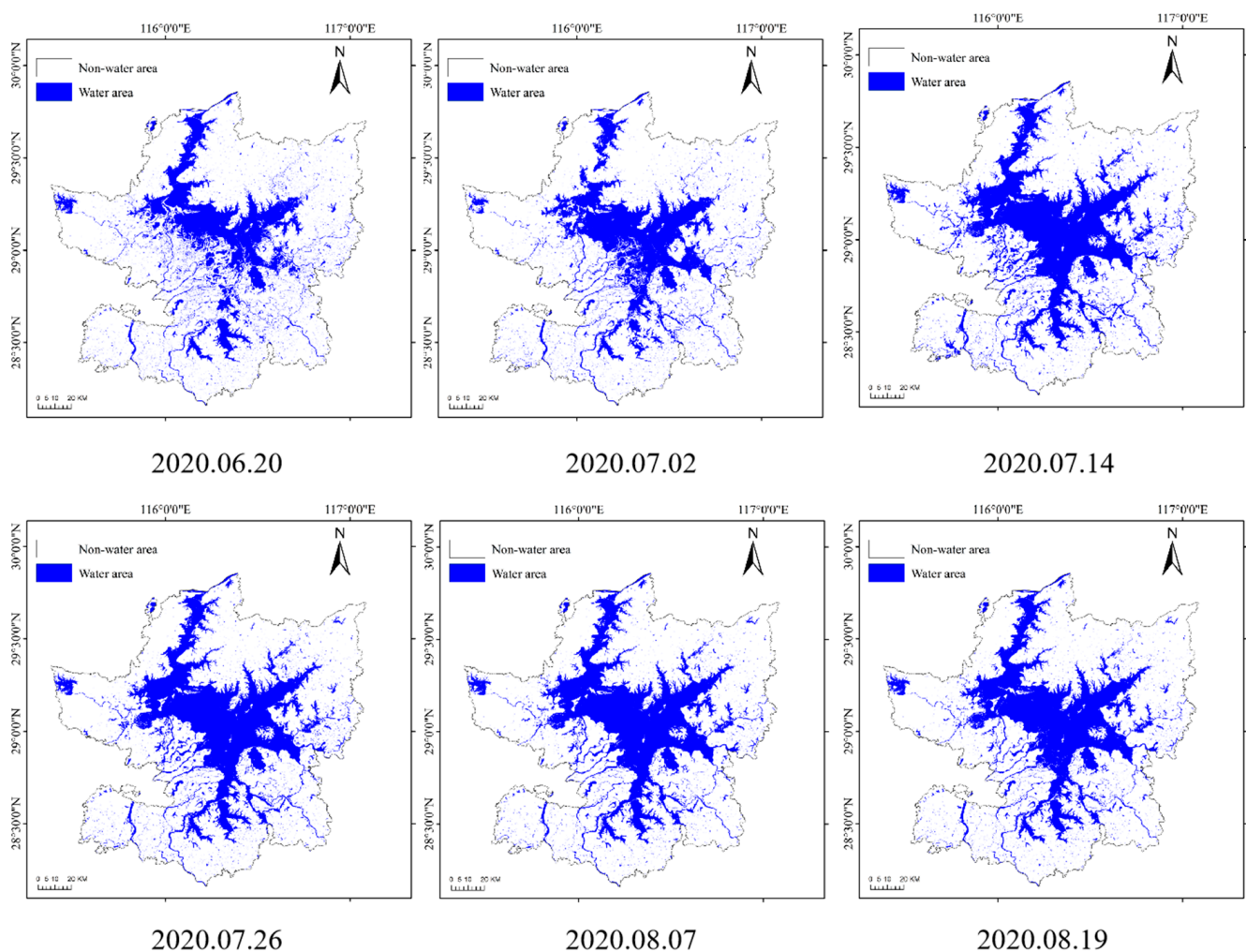

Figure 8. CAU-Net long-time series water extraction results.

This paper took 20 June, 14 July, and 19 August as the pre-flood, mid-flood, and post-flood times, respectively. Figure 10 presents the flood inundation maps determined by overlaying the water body extents during the (i) pre-flood and mid-flood periods; and (ii) the mid-flood and post-flood periods. The maps reveal the severely affected areas of the flood disaster to be concentrated around Poyang Lake, with significant inundation occurring in Yongxiu County, Poyang County, Xinjian District, and Yugan County.
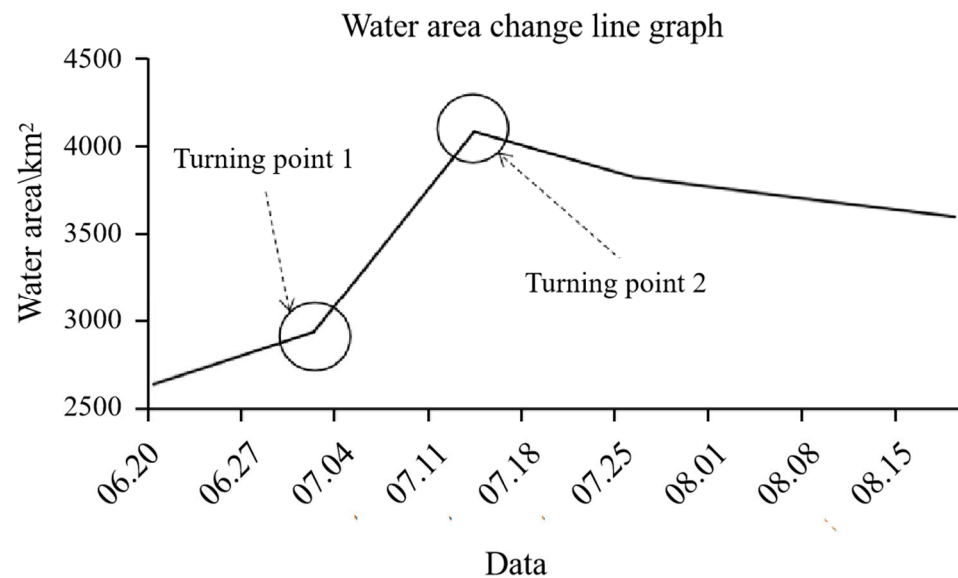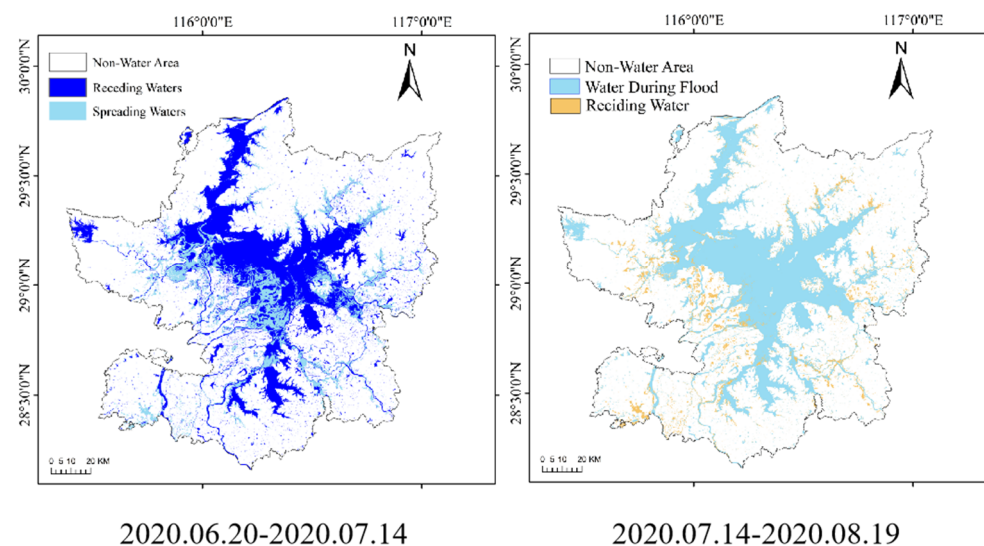
Figure 9. Water area change line chart.

Figure 10. Change of flood inundation extent.

5. Discussion

In the southern regions of China, flood disasters occur frequently during the rainy season every year, causing the inevitable inundation of farmland around lakes and rivers, resulting in significant crop losses. The rapid and accurate acquisition of flood inundation extent and area is of great significance for quick disaster assessments and reducing crop losses. In this study, Sentinel-1 SAR images and SRTM-1 DEM data were employed to compare and analyze three models, namely decision tree, random forest, and CAU-Net. Based on the results, the CAU-Net method was selected to extract the water body extent during the 2020 Poyang Lake flood. The floodwater distribution areas for each period in the study area were subsequently obtained and the disaster situation was analyzed.

The extraction of water body information is critical to remote sensing-based flood monitoring. Optical remote sensing has evolved from simple visual interpretation to the construction of the NDWI, which can achieve relatively accurate water body extraction results, and different water body index layers can be generated under various conditions [33]. However, flood monitoring is distinct to simple water body extraction. During flood disasters, adverse weather conditions often prevail, making optical remote sensing ineffective

for monitoring. Microwave remote sensing, on the other hand, with its ability to penetrate clouds and fog, has become a popular choice for flood monitoring [34]. The results of the three water body extraction methods meet the requirements for high accuracy in terms of the OA and Kappa coefficient. This demonstrates the feasibility of using SAR data for water body extraction, with CAU-Net achieving the highest accuracy.

Numerous shadows are cast by mountains in the study area. Due to their similar characteristics to water bodies in microwave remote sensing images, a considerable number of these mountain shadows are mistakenly identified as water bodies. To obtain a more accurate range of flood disasters, this study proposes three water body extraction methods based on SDWI and terrain features. The results indicate that all three extraction methods effectively suppress the influence of mountain shadows. Among them, by introducing the decision tree method based on SDWI threshold segmentation and conducting a series of experiments, we determined thresholds suitable for terrain features, thus effectively suppressing shadows within water bodies. However, it is worth noting that the segmentation thresholds and classification criteria for this method often rely on the interpreter's experience, resulting in a certain degree of subjectivity. On the other hand, the random forest method does not rely on the prior knowledge of the interpreter, yielding more reasonable extraction results. Our results indicate that the random forest method is more suitable for extracting floodwater bodies in small-scale hilly areas. In comparison, CAU-Net not only reduces the influence of human factors but also achieves high extraction accuracy with the best shadow removal effect on mountainous terrains. Although this method requires time for initial model training, it can be directly applied to multi-temporal flood range extraction in the later stages, making it more efficient. Therefore, the CAU-Net method is undoubtedly more applicable for water body extraction around Poyang Lake, with its extensive mountainous terrain.

The disaster analysis revealed the water area in the Poyang Lake region to exhibit a trend of "rapid expansion and slow recession" during this flood period. On 14 July 2020, the water area reached its peak at 4080 km^2. This flood disaster has caused severe losses, particularly in the heavily affected areas of Yongxiu County, Poyang County, Xinjian District, and Yugan County. The government should prioritize disaster reduction efforts in these regions. It is crucial to scientifically guide the post-disaster recovery of crop production, provide tailored technical support, and minimize disaster losses. In addition, the planning and construction of agricultural infrastructure should be enhanced in these areas. Additional emergency drainage facilities should also be present to prepare for potential rises in water levels or even flooding during future flood seasons, thereby minimizing crop losses.

6. Conclusions

(1) During the rainy season, optical imagery in the southern hilly regions is severely constrained by cloudy and rainy weather conditions. This study effectively addressed this issue by utilizing Sentinel-1 SAR imagery in conjunction with multi-source data. The results demonstrate the feasibility of employing SAR imagery in flood disaster monitoring in the Poyang Lake region, providing a key technological reference for future efforts in flood disaster management.

(2) The deep learning approach demonstrates notable advantages in land feature extraction tasks. With the aim of addressing the issue of interference from mountain shadows in the study area, we propose the CAU-Net method for water body extraction. This method achieves an overall accuracy of 98.71% and a Kappa coefficient of 0.97 in water body extraction within the study area, both of which are at the highest level among the various methods. In the highland areas with abundant mountain shadows, its extraction accuracy reaches 96.45%, representing a significant improvement of 7.09% compared to the SDWI method. CAU-Net effectively facilitates water body extraction in hilly regions. Moreover, it enables the water exaction of long-term image

sequences, thereby realizing the monitoring of flood disaster processes. CAU-Net provides a new technical means for flood monitoring in the Poyang Lake region.

(3) The analysis of long-term image sequences in the study area reveals that the flood area expanded rapidly and subsequently receded slowly. The severely affected areas are primarily located around lakes and rivers, or in relatively low-lying terrain, coinciding with the crop cultivation areas. By analyzing the water body extraction results before and after the flood, this study accurately quantified the flooded area, providing data support for disaster assessments and post-disaster reconstruction.

References

1. *The Ministry of Emergency Management Released the Basic Situation of National Natural Disasters in 2020*; China Disaster Reduction: Beijing, China, 2021; p. 60.
2. *Top Ten Natural Disasters in China in 2020*; China Disaster Reduction: Beijing, China, 2021; p. 60.
3. McFeeters, S.K. The use of the Normalized Difference Water Index (NDWI) in the delineation of open water features. *Int. J. Remote Sens.* **1996**, *17*, 1425–1432. [CrossRef]
4. Duan, J.W.; Zhong, J.S.; Jiang, L.; Zhong, M. Extraction Method of Ultra-Green Water Index for Flood Area After Rain Based on GF-2 Image. *Geogr. Geogr. Inf. Sci.* **2021**, *37*, 35–41.
5. Wu, Q.S.; Wang, M.X.; Shen, Q.; Yao, Y.; Li, J.; Zhang, F.; Zhou, Y. Small water body extraction method based on Sentinel-2 satellite multi-spectral remote sensing image. *Natl. Remote Sens. Bull.* **2022**, *26*, 781–794. [CrossRef]
6. Guo, X.; Zhao, Y.D. Floodinundation Monitoring in Ningxiang of Hunan Province Based on Sentinel-1A SAR. *Remote Sens. Technol. Appl.* **2018**, *33*, 646–656.
7. Zeng, L.F.; Li, L.; Wan, L.H. SAR-based Fast Flood Mapping Using Sentinel-1 Imagery. *Geomat. World* **2015**, *22*, 100–103, 107.
8. Chen, S.N.; Jiang, M. Application Research of Sentinel-1 SAR in Flood Range Extraction and Polarization Analysis. *J. Geo-Inf. Sci.* **2021**, *23*, 1063–1070.
9. Jia, S.C.; Xue, D.J.; Li, C.R. Study on New Method for Water Area Information Extraction based on Sentinel-1 data. *Yangtze River* **2019**, *50*, 213–217.
10. Qiu, J.; Cao, B.; Park, E.; Yang, X.; Zhang, W.; Tarolli, P. Flood Monitoring in Rural Areas of the Pearl River Basin (China) Using Sentinel-1 SAR. *Remote Sens.* **2021**, *13*, 1384. [CrossRef]
11. Tang, L.; Liu, W.; Yang, D.; Chen, L.; Su, Y.; Xu, X. Flooding Monitoring Application Based on the Object-oriented Method and Sentinel-1A SAR Data. *J. Geo-Inf. Sci.* **2018**, *20*, 377–384.
12. Yang, C.J.; Wei, Y.M.; Wang, S.Y. Extracting the Flood Extent from SAR imagery on Basis of DEM. *J. Nat. Disasters* **2002**, *11*, 121–125.
13. Li, F.; Sang, G.Q.; Sun, Y.; Cao, F.J. Research on Methods of Complex Water Body Information Extraction Based on GF-1 Satellite Remote Sensing Data. *J. Univ. Jinan (Sci. Technol.)* **2021**, *35*, 572–579.
14. Pal, M.; Mather, P.M. An assessment of the effectiveness of decision tree methods for land cover classification. *Remote Sens. Environ.* **2003**, *86*, 554–565. [CrossRef]
15. Li, H.K.; Wang, L.J.; Xiao, S.S. Random Forest Classification of Land Use in hilly and mountaineous Area of Southern China Using Multi-source Remote Sensing Data. *Trans. Chin. Soc. Agric. Eng.* **2021**, *37*, 244–251.
16. Zhang, W.C.; Liu, H.B.; Wu, W. Classification of Land Use in Low Mountain and Hilly Area Based on Random Forest and Sentinel-2 Satellite Data: A Case Study of Lishi Town, Jiangjin, Chongqing. *Resour. Environ. Yangtze Basin* **2019**, *28*, 1334–1343.
17. AKollert; Bremer, M.; Loew, M.; Rutzinger, M. Exploring the potential of land surface phenology and seasonal cloud free composites of one year of Sentinel-2 imagery for tree species mapping in a mountainous region. *Int. J. Appl. Earth Obs. Geoinf.* **2021**, *94*, 102208. [CrossRef]

18. Chen, Y.; Fan, R.; Yang, X.; Wang, J.; Latif, A. Extraction of Urban Water Bodies from High-Resolution Remote-Sensing Imagery Using Deep Learning. *Water* **2018**, *10*, 585. [CrossRef]
19. Song, S.; Liu, J.; Liu, Y.; Feng, G.; Han, H.; Yao, Y.; Du, M. Intelligent Object Recognition of Urban Water Bodies Based on Deep Learning for Multi-Source and Multi-Temporal High Spatial Resolution Remote Sensing Imagery. *Sensors* **2020**, *20*, 397. [CrossRef]
20. Zheng, T.H.; Wang, Q.T.; Li, J.G.; Zheng, F.; Zhang, Y.; Zhang, N. Automatic Water Extraction from GF-6 Image Based on Deep Learning. *Sci. Technol. Eng.* **2021**, *21*, 1459–1470.
21. Wang, B.; Chen, Z.L.; Wu, L.; Xie, P.; Fan, D.L.; Fu, B.L. Road extraction of high-resolution satellite remote sensing images in U-Net network with consideration of connectivity. *J. Remote Sens.* **2020**, *24*, 1488–1499. [CrossRef]
22. Wang, X.W.; Zhao, Q.Z.; Tian, W.Z. Influence of U-Net Model on the Accuracy of Shelter Forest Extraction with Different Spatial Resolutions. *Bull. Surv. Mapp.* **2021**, 39–43. [CrossRef]
23. Wang, J.M.; Wang, S.X.; Wang, F.T.; Zhou, Y.; Ji, J.; Xiong, Y.; Wang, Z.; Zhao, Q. Flood inundation region extraction method based on Sentinel-1 SAR data. *J. Catastrophol.* **2021**, *36*, 214–220.
24. Lei, S. Review and Thinking of Poyang Lake Flood in 2020. *Water Resour. Prot.* **2021**, *37*, 7–12.
25. Luan, Y.J.; Guo, J.Y.; Gao, Y.G.; Liu, X. Remote Sensing Monitoring of Flood and Disaster Analysis in Shouguang in 2018 from Sentinel-1B SAR Data. *J. Nat. Disasters* **2021**, *30*, 168–175. [CrossRef]
26. Zhang, D.Y.; Dai, Z.; Xu, X.G.; Yang, G.; Meng, Y.; Feng, H.; Hong, Q.; Jiang, F. Crop Classification of Modern Agricultural Park Based on Time-series Sentinel-2 Images. *Infrared Laser Eng.* **2021**, *50*, 262–272.
27. Breiman, L. Random forests. *Mach. Learn.* **2001**, *45*, 5–32. [CrossRef]
28. Zhao, X.; Tian, B.; Niu, Y.; Chen, C.; Zhou, Y. Classification of coastal salt marsh based on Sentinel-1 time series backscattering characteristics: The case of the Yangtze River delta. *J. Remote. Sens.* **2022**, *26*, 672–682. [CrossRef]
29. Yang, S.; Li, D.; Yan, L.; Huang, Y.; Wang, M. Landslide Susceptibility Assessment in High and Steep Bank Slopes Along Wujiang River Based on Random Forest Model. *Saf. Environ. Eng.* **2021**, *28*, 131–138. [CrossRef]
30. Ronneberger, O.; Fischer, P.; Brox, T. U-Net: Convolutional Networks for Biomedical Image Segmentation. *arXiv* **2015**, arXiv:1505.04597. Available online: http://arxiv.org/abs/1505.04597 (accessed on 27 July 2023).
31. Dong, Z.; Wang, G.; Amankwah, S.O.Y.; Wei, X.; Feng, A. Monitoring the summer flooding in the Poyang Lake area of China in 2020 based on Sentinel-1 data and multiple convolutional neural networks. *Int. J. Appl. Earth Obs. Geoinf.* **2021**, *102*, 102400. [CrossRef]
32. Ning, X.-G.; Chang, W.-T.; Wang, H.; Zhang, H.; Zhu, Q. Extraction of marsh wetland in Heilongjiang Basin based on GEE and multi-source remote sensing data. *Natl. Remote Sens. Bull.* **2022**, *26*, 386–396. [CrossRef]
33. Li, L.; Su, H.; Du, Q.; Wu, T. A novel surface water index using local background information for long term and large-scale Landsat images. *ISPRS J. Photogramm. Remote Sens.* **2021**, *172*, 59–78. [CrossRef]
34. Njoku, E.G.; Moghaddam, M.; Moller, D.; Molotch, N. Microwave Remote Sensing for Land Hydrology Research and Applications: Introduction to the Special Issue. *IEEE J. Sel. Top. Appl. Earth Obs. Remote Sens.* **2010**, *3*, 3–5. [CrossRef]